Advances in electron channelling contrast imaging and electron backscatter diffraction for imaging and analysis of structural defects in the scanning electron microscope

IOP Conf. Series: Materials Science and Engineering **891** (2020) 012023 doi:10.1088/1757-899X/891/1/012023

Advances in electron channelling contrast imaging and electron backscatter diffraction for imaging and analysis of structural defects in the scanning electron microscope

C Trager-Cowan[1], A Alasmari[1], W Avis[1], J Bruckbauer[1], P R Edwards[1], B Hourahine[1], S Kraeusel[1], G Kusch[1], B M Jablon[1], R Johnston[1], R W Martin[1], R McDermott[1], G Naresh-Kumar[1], M Nouf-Allehiani[1], E Pascal[1], D Thomson[1], S Vespucci[1], K Mingard[2], P J Parbrook[3], M D Smith[3], J Enslin[4], F Mehnke[4], M Kneissl[4,5], C Kuhn[4], T Wernicke[4], A Knauer[5], S Hagedorn[5], S Walde[5], M Weyers[5], P-M Coulon[6], P A Shields[6], Y Zhang[7], L Jiu[7], Y Gong[7], R M Smith[7], T Wang[7] and A Winkelmann[1,8]

[1] University of Strathclyde, Department of Physics, SUPA, Glasgow G4 0NG, Great Britain
[2] National Physics Laboratory, Teddington TW11 0LW, Great Britain
[3] University College Cork, Tyndall National Institute, Cork T12 R5CP, Ireland
[4] Technische Universität Berlin, Institut für Festkörperphysik, 10623 Berlin, Germany
[5] Leibniz-Institut für Höchstfrequenztechnik, Ferdinand-Braun-Institut, 12489 Berlin, Germany
[6] University of Bath, Department of Electronic and Electrical Engineering, Bath BA2 7AY, Great Britain
[7] University of Sheffield, Department of Electronic and Electrical Engineering, Sheffield S1 3JD, Great Britain
[8] AGH - University of Science and Technology, Academic Centre for Materials and Nanotechnology (ACMiN), 30059 Krakow, Poland

E-mail: c.trager-cowan@strath.ac.uk

Abstract. In this article we describe the scanning electron microscopy (SEM) techniques of electron channelling contrast imaging and electron backscatter diffraction. These techniques provide information on crystal structure, crystal misorientation, grain boundaries, strain and structural defects on length scales from tens of nanometres to tens of micrometres. Here we report on the imaging and analysis of dislocations and sub-grains in nitride semiconductor thin films (GaN and AlN) and tungsten carbide-cobalt (WC-Co) hard metals. Our aim is to illustrate the capability of these techniques for investigating structural defects in the SEM and the benefits of combining these diffraction-based imaging techniques.

1. Introduction

The scanning electron microscope (SEM) is a very powerful tool for investigating and imaging a wide range of material properties spanning topography, structure, composition and light emission [1-4].

SEMs are extensively used for imaging topography by monitoring the intensity of secondary electrons as a focussed electron beam, with an energy in the range of 100 eV to 30 keV, is rastered over the surface of a sample. Less well known are the techniques of electron channelling contrast imaging (ECCI) [5-14] and electron backscatter diffraction (EBSD) [5-6, 14-20], which exploit diffraction to provide information on crystal structure, crystal misorientation, grain boundaries, strain and structural defects such as dislocations and stacking faults. Here we provide an overview of these techniques and illustrate their application by describing some of our recent investigations of the structural properties of nitride semiconductor thin films (GaN and AlN) and WC-Co hard metals.

To carry out our measurements we use a range of SEMs equipped with both commercial and bespoke detection systems. In the work reported here we have used an FEI Sirion 200 Schottky field emission gun SEM (Sirion SEM) equipped with an in-house developed ECCI system. We have also used an FEI Quanta 250 Schottky field emission gun environmental/variable pressure SEM (Quanta SEM) equipped with gaseous electron detectors for electron detection when the SEM is used in low vacuum or environmental modes. The Quanta SEM is also equipped with an Oxford Instruments Nordlys EBSD detector and forescatter diodes for EBSD and ECCI measurements respectively. The ability to vary the chamber pressure in the Quanta SEM allows the dissipation of charge and therefore imaging of high resistivity materials such as AlN.

2. The electron backscatter diffraction (EBSD) and electron channelling contrast imaging techniques (ECCI)

ECCI and EBSD both exploit diffraction to reveal the structural properties of the crystalline material under investigation. For ECCI it is diffraction of the incident beam which provides the greatest contrast in the resultant images, while for EBSD it is diffraction of backscattered electrons which provide the crystallographic information. The spatial and depth resolution of both techniques is of the order of tens of nanometres. For successful imaging using either ECCI or EBSD, the sample needs to have a reasonably smooth and clean surface. For the imaging of metal surfaces or the surfaces of geological specimens this usually requires careful sample polishing to produce a high quality surface [10], this is also the case for semiconductor wafers cut from bulk crystals. However, for most epitaxially grown semiconductor thin films no surface preparation is required.

2.1. Electron channelling contrast imaging (ECCI)

ECCI micrographs may be produced when a sample is placed so that a plane or planes are at, or close to, the Bragg angle with respect to the incident electron beam. Any deviation in crystallographic orientation or in lattice constant due to local strain will produce a variation in contrast in the resultant ECCI micrograph. The micrograph is constructed by monitoring the intensity of backscattered or forescattered electrons as the electron beam is scanned over the sample. Extremely small changes in orientation and strain are detectable, revealing, for example, low angle tilt and rotation boundaries and atomic steps. Extended defects such as dislocations and stacking faults may also be imaged [5-14, 21-29]. The conditions required to resolve individual dislocations in an electron channelling contrast image are quite stringent: an electron beam with a small spot size (nanometres), high brightness (nanoamps or higher) and low divergence (a few mrad) is required [5, 30]. Such conditions are met in a field emission gun SEM. The ECCI micrographs shown in this paper were acquired at 20 - 30 keV and we show ECCI micrographs where dislocations of order 80 nm apart can be resolved. ECCI micrographs can be acquired at lower electron beam energies, for example see refs. [29] and [31]. In ref. [29] the smallest size of the investigated 3D structures revealed in their ECCI micrographs was 28 nm. While ECCI is an excellent technique for revealing and quantifying defects which reach the surface, and we show some example results in sections 3.1 and 3.3, it is harder to quantify dislocations below the surface due to the surface sensitivity of the ECCI technique and the difficulty in determining its precise sampling depth. Some control of the sampling depth can be achieved by changing the electron beam energy. It is possible to obtain quantitative data on dislocations which lie below the surface, as

illustrated for example by the paper by Carnevale *et al.* [22] on misfit dislocations in GaP. They were able to image dislocations lying at up to around 100 nm from the surface, where they acquired ECCI micrographs at a beam energy of 25 keV in the backscatter geometry (see discussion below).

Figure 1 illustrates the two geometries, namely the backscatter and forescatter geometries which are used to acquire ECCI micrographs. The backscatter geometry (Fig. 1a) has the advantage that this geometry does not require a high tilt of the sample and, therefore, a significant correction of the image to account for tilt is not required. This geometry also allows the easiest imaging of large samples, for example full semiconductor wafers. The forescatter geometry (Fig. 1b) has the advantage that images exhibit better signal-to-noise compared to the backscatter geometry due to the increase in intensity of backscattered electrons. The detector used to detect the backscattered electrons is generally an electron-sensitive diode. Key to the acquisition of good quality ECCI micrographs is the use of a good amplification system. An amplifier with a large DC offset and high small signal gain greatly facilitates the acquisition of ECCI micrographs.

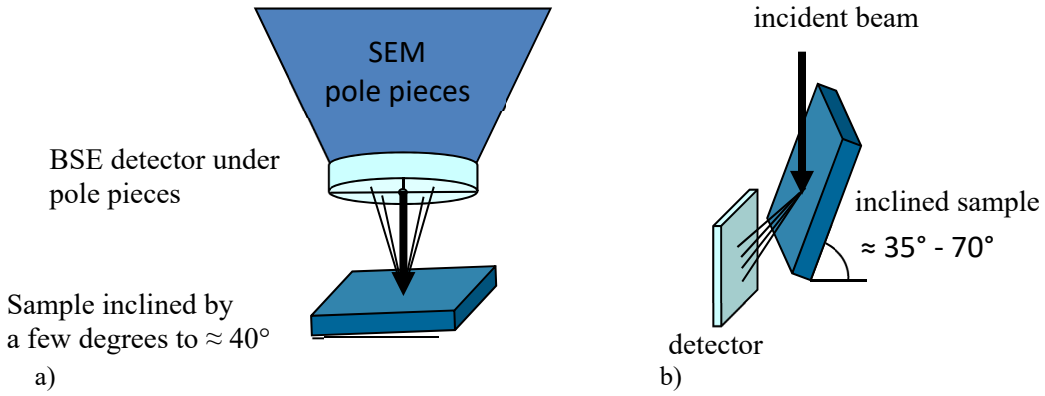

Figure 1. Illustrating the a) backscatter, and b) forescatter geometries for acquisition of ECCI micrographs [reproduced from 32].

2.2. Electron backscatter diffraction (EBSD)

In EBSD the sample is tilted at around 70° to the normal of the incident electron beam. The impinging electrons are scattered inelastically through high angles forming a diverging source of electrons, which can be diffracted. The resultant electron backscatter pattern (EBSP) consists of a large number of overlapping bands, known as Kikuchi bands, which are closely related to a 2D projection of the crystal structure, where each Kikuchi band corresponds to a set of planes, as illustrated in Fig. 2b. EBSPs are generally detected by an electron sensitive phosphor or scintillator screen and a charge-coupled device (CCD) or complementary metal-oxide semiconductor (CMOS) camera [15] (see Fig. 2a), although there have been recent developments of direct electron cameras [33-34]. The EBSP shown in Fig. 2b was acquired at 20 keV from a Si sample using energy-filtered direct electron detection with a collection angle of ≈ 50°. Direct electron detection allows high quality EBSPs to be acquired at low electron beam energies and pattern acquisition down to 3 keV is achievable [30]. EBSD is a well-established technique for texture analysis and for quantifying grain boundaries and crystal phases [5-6, 14-20]. The introduction of cross-correlation based analysis of EBSPs has also made possible measurements of relative strain, geometrically necessary dislocations, and lattice tilt and twist [16, 35], antiphase domains [36] and crystal polarity [37-38].

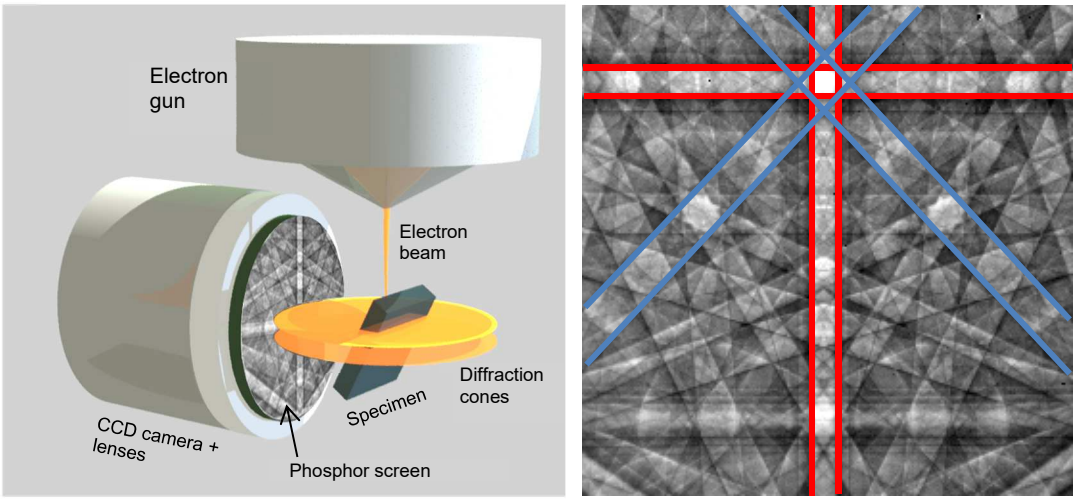

a) b)

Figure 2. a) Illustration of the EBSD detection geometry and a conventional EBSD detector, and b) an EBSP from Si acquired at an energy of 20 keV with a collection angle of ≈ 50°. The red lines outline Kikuchi bands corresponding to {200} planes, the blue lines outline Kikuchi bands corresponding to {220} planes. Adapted from [34] under Creative Commons Attribution (CC BY) license: http://creativecommons.org/licenses/by/4.0/.

3. Example results

3.1. The use of ECCI to image sub-grains and dislocations in a GaN thin film

Figure 3a shows an ECCI micrograph of a GaN thin film grown on *c*-plane sapphire by metalorganic vapour phase epitaxy (MOVPE). The ECCI micrograph was acquired at an electron beam energy of 30 keV in the forescatter geometry in the Sirion SEM. The variation in grey scale in the ECCI micrograph is a result of small differences in orientation of sub-grains in the thin film. This is highlighted in the pseudo-colour image in Fig. 3b. The "spots" in the image, most of which exhibit a black-white contrast (see inset of Fig. 3a for example), are threading dislocations; that is dislocations which thread through the thin film to the surface and are caused by the growth on the lattice-mismatched sapphire substrate. The threading dislocations propagate to the surface of the sample and are revealed due to associated strain fields [39]. For this GaN thin film the average threading dislocation density was determined to be $\approx 3 \times 10^8$ cm^{-2}. A large number of the threading dislocations are seen to lie on sub-grain boundaries. Note that in order to reveal all misorientations, and thus all the sub-grain boundaries, a number of ECCI micrographs need to be acquired under a range of diffraction conditions [40]. To select a particular diffraction condition, that is to select the plane or planes from which the incident electron beam will be diffracted (usually referred to as selecting the g-vector), it is necessary to acquire an electron channelling pattern (ECP). This is discussed in Section 3.2. While the contrast in the ECCI micrograph reveals the presence of sub-grains, it does not provide any quantitative information on their orientation. The magnitude and direction of misorientation can be measured by EBSD, and an EBSD study of sub-grain orientations for an AlN thin film is presented in Section 3.3.

3.2. Selection/determination of the diffraction condition for ECCI, acquiring ECPs

An ECP is obtained when changes in the backscattered electron intensity are recorded as the angle of the incident electron beam is changed relative to the surface of a single crystal area of the sample. When the beam changes its angle with respect to the sample, different planes of the crystal satisfy the Bragg condition, giving rise to the appearance of overlapping Kikuchi bands superimposed on the image of the

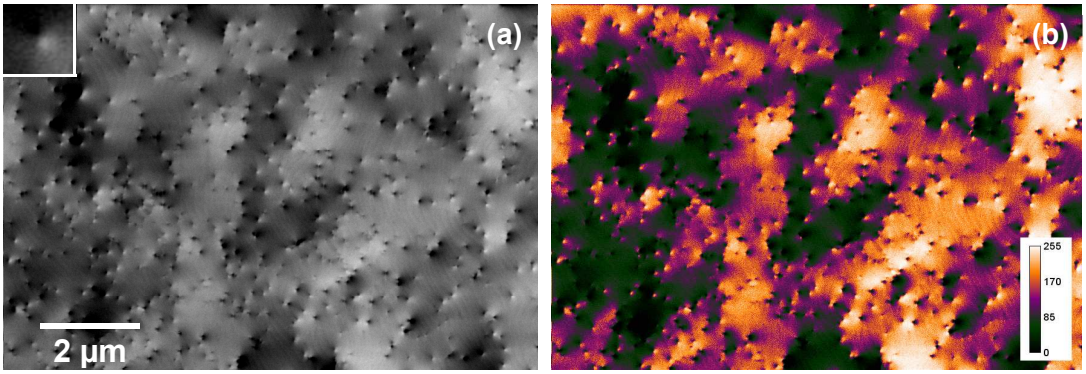

Figure 3. ECCI micrograph from a GaN thin film presented as a) a grey scale image, and b) a pseudo-colour image.

sample; an ECP from a GaN thin film is shown in Fig. 4. The ECP, like an EBSP (the two are related by reciprocity), is closely related to the 2D projection of the crystal structure, with the Kikuchi bands corresponding to different planes in the crystal. Comparing the ECP with kinematical and/or dynamical electron diffraction simulations allows the pattern to be indexed, i.e., the planes in the ECP can be identified. In this case Fig. 4a shows a dynamical simulation [41] and illustrates the detail achievable in such simulations, such detail can greatly facilitate the indexing of the ECP. Figure 4c is a kinematical simulation (produced with ESPRIT DYNAMICS (Bruker Nano) software) and is included to highlight the indices of some of the planes giving rise to the Kikuchi bands observed in the ECP. The plane (or planes) which intersect the centre of the ECP, usually referred to as the pattern centre (PC), are those from which the incident electron beam is diffracted. In the example shown in Fig. 4, the incident electron beam was diffracted from one of the {11-20} planes; so the **g**-vector is one of {11-20}.

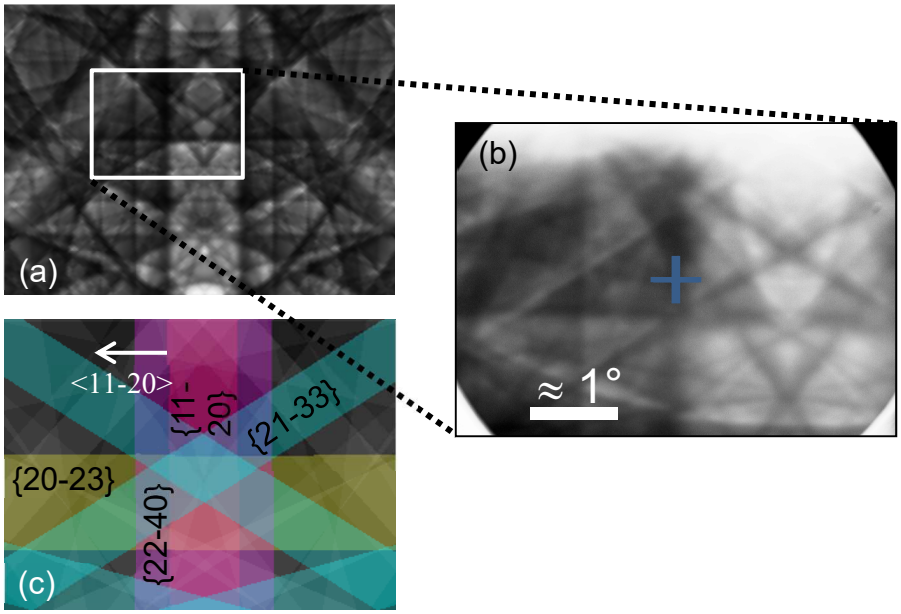

Figure 4. a) Dynamical simulation of an electron channelling pattern (ECP) from a GaN thin film. Electron beam energy is 30 keV, sample tilt ≈ 40°. b) Experimental ECP. The blue cross marks the pattern centre (PC). c) Kinematical simulation of the ECP with some indexed planes highlighted (produced with ESPRIT DYNAMICS (Bruker Nano) software). In this case the PC intersects with the edge one of the {11-20} Kikuchi bands; so the **g**-vector is one of {11-20}. [Reproduced from 32].

An ECP may be obtained by acquiring a backscattered image at low magnification. At low magnification, as the beam is scanned over the sample, it changes its angle with respect to the surface of the sample (in our case, for our Sirion SEM, this is by around ±2.5°), leading to the formation of an ECP [9]. Note that this method of acquiring an ECP is only possible if the scanned area of the sample (of order 5 mm × 5 mm in size) is smooth and all of the same crystallographic orientation. An ECCI micrograph is obtained on zooming in on the PC by increasing the magnification. At higher magnification the beam has a fixed angle with respect to the sample surface as the beam is scanned. The resultant ECCI micrograph will reveal any defects which distort the plane or planes which correspond to the Kikuchi bands intersecting the PC. Alternatively, if 'beam rocking' electron optics are available in the SEM, the angle of the beam with respect to the sample can be changed over a much smaller surface area. Selected area ECPs, referred to as SAECPS or SACPs can be acquired from areas ranging from 10 µm × 10 µm down to of order 500 nm × 500 nm in size [42]. While a lot of useful information can be obtained from ECCI without the acquisition of ECPs, the ability to acquire ECPs makes ECCI far more powerful and easier to use, in particular when it is applied to the identification of unknown extended defects such as dislocations and stacking faults.

3.3. The use of ECCI and EBSD to investigate sub-grains and dislocations in a c-plane AlN thin film

Figure 5 shows ECCI micrographs and EBSD maps from a *c*-plane AlN thin film overgrown by MOVPE on a nano-patterned sapphire substrate (nPSS). For this sample the sapphire substrate has a 0.1° offcut towards the sapphire *m*-plane. The experiments were performed in the Quanta SEM operated in low vacuum mode (0.5 mbar) to avoid charging of the insulating AlN sample.

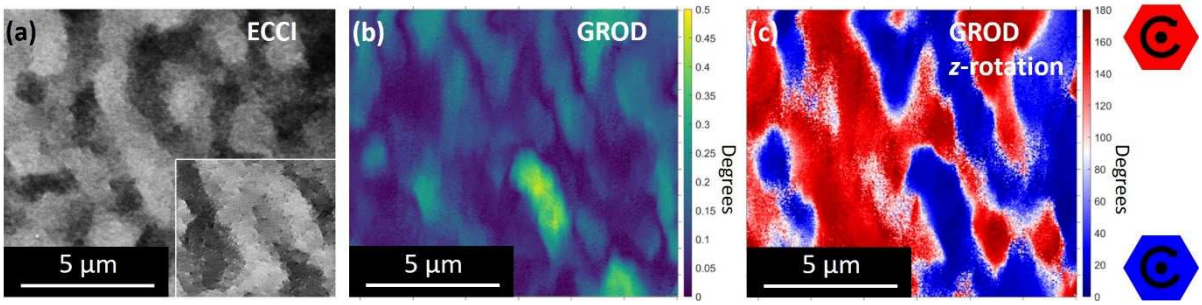

Figure 5. ECCI micrographs and EBSD maps from a *c*-plane AlN thin film. a) ECCI micrograph, acquired at an electron beam energy of 25 keV, revealing sub-grains. The inset shows a higher resolution ECCI micrograph revealing threading dislocations ("spots" exhibiting black-white contrast). b) Grain reference orientation deviation (GROD) map, and c) GROD *z*-rotation map where the colours denote direction of rotation around the *c*-axis. The red regions are rotated in the opposite direction to the blue regions as indicated by the blue and red hexagons. The GROD and GROD *z*-rotation maps were derived from EBSD data acquired at 20 keV. Note that the ECCI micrograph and EBSD maps were acquired from the same sample, but not from the same area of the sample. Adapted from [45] under Creative Commons Attribution (CC BY) license: http://creativecommons.org/licenses/by/4.0/.

The contrast in the ECCI micrograph of Fig. 5a is a result of small differences in orientation of sub-grains in the thin film. The inset shows a higher resolution ECCI micrograph where threading dislocations propagating to the surface of the sample are revealed; the threading dislocation density was determined to be 1.5×10^9 cm^{-2}. A significant number of the threading dislocations are located on the sub-grain boundaries. As stated previously in Section 3.1, while ECCI reveals differences in orientation between sub-grains, it does not provide a measure of the magnitudes and directions of these

misorientations. Figure 5b shows a grain reference orientation deviation (GROD) map, the deviation of orientation of the sub-grains relative to a reference orientation [17]. In this case the reference orientation is the *c*-direction; that is the [0001] direction. The GROD map was produced from EBSD data using MTEX [43]. The first step of the analysis involved comparison of each EBSP with dynamical simulations [41]. This pattern matching approach was used in the EBSD analysis as it substantially improves orientation precision [44]. Figure 5c is a GROD *z*-rotation map showing the rotation of the sub-grains with respect to the nominal sample normal, i.e., around the *c*-axis. The colours, blue and red, denote the direction of this in-plane rotation. The red regions are rotated in the opposite direction to the blue regions.

The results presented above illustrate how ECCI and EBSD can provide complementary structural information. ECCI allows fast determination of dislocation densities and their distribution and reveals the presence of sub-grains. Figure 5 and its inset each took around 10 minutes of direct acquisition. EBSD provides quantitative information on the magnitude and direction of the misorientations in the film. However the EBSD data from which the maps of Fig. 5 were derived, took of order three hours to acquire. The EBSD data acquisition was then followed by further data analysis which is also time-consuming. In spite of this, both techniques share the advantages of being non-destructive and can be used to interrogate large areas of a sample.

3.4. The use of ECCI and EBSD to investigate sub-grains in an as-sintered WC-Co hard metal sample

Figures 6a to 6c show an ECCI micrograph, a GROD map and a GROD axis map from WC grains of an as-sintered WC-Co hard metal sample. The sample was first mechanically polished to an optical finish using standard metallographic techniques, finishing with a colloidal silica polish, which leaves a mirror finish and no visible scratches on the surface. It was also further polished in a Hitachi IM4000 argon ion beam polishing system to remove any fine scratches due to the mechanical polishing. This created a polished surface ready for examination in the SEM. While producing a scratch free surface, ion beam polishing induces shallow (of the order of 10 nm) dimples in the WC grains despite rotation under the ion beam to even out variation in milling rate with grain orientation: these dimples need to be taken into account when analysing the acquired data.

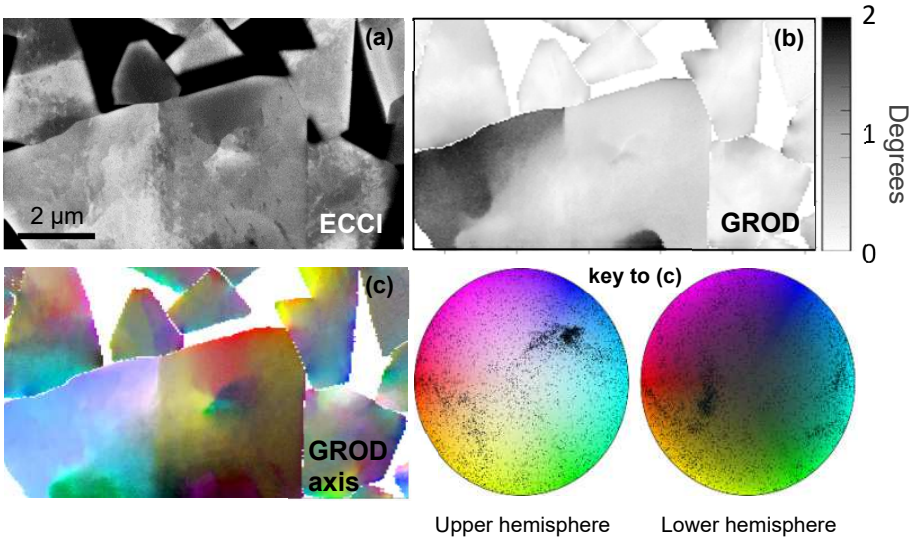

Figure 6. ECCI and EBSD maps from WC grains of an as-sintered WC-Co hard metal. a) ECCI micrograph acquired at 20 keV, b) GROD map, and c) a GROD axis map. The GROD and GROD axis maps were derived from EBSD data acquired at 20 keV. Note in this case the ECCI micrograph and EBSD maps were acquired from the same area of the sample. Reprinted in part from [46] with permission from Elsevier.

For the GROD axis map each pixel has a value denoting the rotation axis with respect to the mean axis for that grain, as defined by the colour key to the right of the image. The ECCI micrograph and EBSD maps reveal sub-grains within nominally single crystal WC grains, indicating how the large grains may have evolved during the sintering process. ECCI also reveals dislocations within the WC grains [46]. In this case the EBSD derived maps again provide quantification of the sub-grain misorientations; the GROD axis map reveals the misorientations are around more than one axis. The colour key indicates the direction of the misorientation axes in real space above (upper hemisphere) or below (lower hemisphere) the sample. The black dots indicate these directions for each point in the map.

4. Summary

To summarise, we have shown that ECCI allows direct, fast imaging of dislocations and sub-grain boundaries, while EBSD provides quantitative information on the magnitude and direction of misorientations in the sample. Both techniques share the advantages of being non-destructive and can be used to interrogate and provide valuable, complementary information on defects and crystallographic properties from large areas of a sample.

Acknowledgements

The authors would like to acknowledge financial support of the EPSRC, UK via Grant No. EP/M015181/1, "Manufacturing nano-engineered III-nitrides"; and Grant No. EP/P015719/1, "Quantitative non-destructive nanoscale characterisation of advanced materials". Data associated with this research are available at https://doi.org/10.15129/b5238863-a088-4f30-8b13-2625260eb73a [45] and https://doi.org/10.15129/c80a3a0c-a718-4941-ac82-8981d21799ce [46], or from the corresponding author.

References

[1] Holt D B and Joy D C (Eds.) 1989 *SEM microcharacterization of semiconductors*. (Cambridge, UK: Academic Press).
[2] Goldstein J, Newbury D, Joy D, Lyman C, Echlin P, Lifshin E, Sawyer L and Michael J 2007 *Scanning electron microscopy and X-ray microanalysis*. (Boston, MA: Springer)
[3] Reimer L 1998 *Scanning electron microscopy: Physics of image formation and microanalysis*. (Berlin-Heidelberg, Germany: Springer)
[4] Zhou W and Wang Z L 2007 *Scanning microscopy for nanotechnology: techniques and applications*. (Boston, MA: Springer Science & Business Media)
[5] Wilkinson A J and Hirsch P B 1997 Electron diffraction based techniques in scanning electron microscopy of bulk materials. *Micron* **28** 279-308
[6] Trager-Cowan C, Sweeney F, Trimby P W, Day A P, Gholinia A, Schmidt N H, Parbrook P J, Wilkinson A J and Watson I M 2007 Electron backscatter diffraction and electron channeling contrast imaging of tilt and dislocations in nitride thin films. *Phys. Rev. B.* **75** 085301
[7] Crimp M A, Simkin B A and Ng B C 2001 Demonstration of the g·bxu=0 edge dislocation invisibility criterion for electron channelling contrast imaging. *Philos. Mag. Lett.* **81** 833-837
[8] Picard Y, Kamaladasa R, De Graef M, Nuhfer N, Mershon W, Owens T, Sedlacek L and Lopour F 2012 Future prospects for defect and strain analysis in the SEM via electron channeling. *Micros. Today* **20** (2) 12-16
[9] Naresh-Kumar G, Hourahine B, Edwards P R, Day A P, Winkelmann A, Wilkinson A J, Parbrook P J, England G and Trager-Cowan C 2012 Rapid nondestructive analysis of threading dislocations in wurtzite materials using the scanning electron microscope. *Phys. Rev .Lett.* **108** 135503
[10] Zaefferer S and Elhami N N 2014 Theory and application of electron channelling contrast imaging under controlled diffraction conditions. *Acta Mater.* **75** 20-50

[11] Deitz J I, Carnevale S D, Ringel S A, McComb D W and Grassman T J 2015 Electron channeling contrast imaging for rapid III-V heteroepitaxial characterization. *J. Vis. Exp.* **101** e52745
[12] Naresh-Kumar G, Thomson D, Nouf-Allehiani M, Bruckbauer J, Edwards P R, Hourahine B, Martin R W and Trager-Cowan C 2016 Electron channelling contrast imaging for III-nitride thin film structures. *Mater. Sci. Semicond. Process.* **47** 44-50
[13] L'Hôte G, Lafond C, Steyer P, Deschanel S, Douillard T, Langlois C and Cazottes S 2019 Rotational-electron channeling contrast imaging analysis of dislocation structure in fatigued copper single crystal. *Scripta Materialia* **162** 103-107
[14] Brodusch N, Demers H and Gauvin R 2018 Electron diffraction techniques in the SEM. in: *Field emission scanning electron microscopy*. (Singapore: Springer) Springer Briefs in Applied Sciences and Technology
[15] Schwartz A J, Kumar M, Adams B L and Field D P 2009 *Electron backscatter diffraction in materials science*. (Berlin, Germany: Springer)
[16] Wilkinson A J and Britton T B 2012 Strains, planes, and EBSD in materials science. *Mater. Today* **15** 366-376
[17] Wright S I, Nowell M M and Field D P 2011 A review of strain analysis using electron backscatter diffraction. *Microsc. Microanal.* **3** 316-329
[18] Wright S I, Nowell M M, de Kloe R, Camus P and Rampton T 2015 Electron imaging with an EBSD detector. *Ultramicroscopy* **148** 132-145
[19] Moussa C, Bernacki M, Besnard R and Bozzolo N 2017 Statistical analysis of dislocations and dislocation boundaries from EBSD data. *Ultramicroscopy* **179** 63-72
[20] Brodusch N, Demers H and Gauvin R 2018 Imaging with a commercial electron backscatter diffraction (EBSD) camera in a scanning electron microscope: A review. *J. Imaging* **4** 88
[21] Naresh-Kumar G, Mauder C, Wang K R, Kraeusel S, Bruckbauer J, Edwards P R, Hourahine B, Kalisch H, Vescan A, Giesen C and Heuken M 2013 Electron channeling contrast imaging studies of nonpolar nitrides using a scanning electron microscope. *Appl. Phys. Lett.* **102** 142103
[22] Carnevale S D, Deitz J I, Carlin J A, Picard Y N, De Graef M, Ringel S A and Grassman T J 2014 Rapid misfit dislocation characterization in heteroepitaxial III-V/Si thin films by electron channeling contrast imaging. *Appl. Phys. Lett.* **104** 232111
[23] Hite J K, Mastro M A and Eddy Jr C R 2010 Approach for dislocation free GaN epitaxy. *J. Cryst. Growth* **312** 3143-3146
[24] Schulze A, Strakos L, Vystavel T, Loo R, Pacco A, Collaert N, Vandervost W and Caymax M 2018 Non-destructive characterization of extended crystalline defects in confined semiconductor device structures. *Nanoscale* **10** 7058-7066
[25] Callahan P G, Haidet B B, Jung D, Seward G G and Mukherjee K 2018 Direct observation of recombination-enhanced dislocation glide in heteroepitaxial GaAs on silicon. *Phys. Rev. Mater.* **2** 081601
[26] Yaung K N, Kirnstoetter S, Faucher J, Gerger A, Lochtefeld A, Barnett A and Minjoo L L 2016 Threading dislocation density characterization in III–V photovoltaic materials by electron channeling contrast imaging. *J. Cryst. Growth* **453** 65-70
[27] Kaboli S and Burnley P C 2018 Direct observations of crystal defects in polycrystalline diamond. *Mater. Characterization* **142** 154-161
[28] Miyajima N, Li Y, Abeykoon S and Heidelbach F 2018 Electron channelling contrast imaging of individual dislocations in geological materials using a field-emission scanning electron microscope equipped with an EBSD system. *Eur. J. Mineral.* **30** 5-15
[29] Han H, Hantschel T, Strakos L, Vystavel T, Baryshnikova M, Mols Y, Kunert B, Langer R, Vandervorst W and Caymax M 2020 Application of electron channeling contrast imaging to 3D semiconductor structures through proper detector configurations. *Ultramicroscopy* **210** 112928
[30] Joy D C, Newbury D E and Davidson D L 1982 Electron channeling patterns in the scanning electron microscope. *J. Appl. Phys.* 53 R81-122

[31] Naresh-Kumar G, Trager-Cowan C and Mingard K P 2019 Electron channelling contrast imaging in a low voltage scanning electron microscope. *Microsc. Microanal.* **25** 504-505
[32] Massabuau F C-P, Bruckbauer J, Trager-Cowan C and Oliver R A 2019 Chapter 8: Microscopy of defects in semiconductors. in: Characterisation and control of defects in semiconductors. (Tuomisto F; Ed.) (London, UK: IET)
[33] Wilkinson A J, Moldovan G, Britton T B, Bewick A, Clough R and Kirkland A I 2013 Direct detection of electron backscatter diffraction patterns. *Phys. Rev. Lett.* **111** 065506
[34] Vespucci S, Winkelmann A, Naresh-Kumar G, Mingard K P, Maneuski D, Edwards P R, Day A P, O'Shea V and Trager-Cowan C 2015 Digital direct electron imaging of energy-filtered electron backscatter diffraction patterns. *Phys. Rev. B* **92** 205301
[35] Wilkinson A J, Meaden G and Dingley D J 2006 High-resolution elastic strain measurement from electron backscatter diffraction patterns: new levels of sensitivity. *Ultramicroscopy* **106** 307-313
[36] Naresh-Kumar G, Vilalta-Clemente A, Jussila H, Winkelmann A, Nolze G, Vespucci S, Nagarajan S, Wilkinson A J and Trager-Cowan C 2017 Quantitative imaging of anti-phase domains by polarity sensitive orientation mapping using electron backscatter diffraction. *Sci. Rep.* **7** 10916
[37] Winkelmann A, Nolze G, Himmerlich M, Lebedev V and Reichmann A 2016 Point-group sensitive orientation mapping using EBSD. in: Proc. 6th Int. Conf. Recrystallization and Grain Growth. (Holm E A, Farjami S, Manohar P, Rohrer G, Rollett A D, Srolovitz D and Weiland H; Eds.) (Berlin-Heidelberg, Germany: Springer) 281-286
[38] Naresh-Kumar G, Bruckbauer J, Winkelmann A, Yu X, Hourahine B, Edwards P R, Wang T, Trager-Cowan C and Martin R W 2019 Determining GaN nanowire polarity and its influence on light emission in the scanning electron microscope. *Nano Lett.* **19** 3863-3870
[39] Pascal E, Hourahine B, Naresh-Kumar G, Mingard K and Trager-Cowan C 2018 Dislocation contrast in electron channelling contrast images as projections of strain-like components. *Mater. Today: Proceedings* **5** 14652-14661
[40] Day A P and Quested T E 1999 A comparison of grain imaging and measurement using horizontal orientation and colour orientation contrast imaging, electron backscatter pattern and optical methods. *J. Microscopy* **195** 186-196
[41] Winkelmann A, Trager-Cowan C, Sweeney F, Day A P and Parbrook P J 2007 Many-beam dynamical simulation of electron backscatter diffraction patterns. *Ultramicroscopy* **107** 414-421
[42] Mansour H, Guyon J, Crimp M A, Gey N, Beausir B and Maloufi A N 2014 Accurate electron channeling contrast analysis of dislocations in fine grained bulk materials. *Scripta Materialia* **84** 11-14
[43] Bachmann F, Hielscher R and Schaeben H 2010 Texture analysis with MTEX - Free and open source software toolbox. *Solid State Phenomena* **160** 63-68
[44] Winkelmann A, Jablon B M, Tong V S, Trager-Cowan C and Mingard K P 2020 Improving EBSD precision by orientation refinement with full pattern matching. *J. Microscopy* **277** 79-92
[45] Trager-Cowan C, Alasmari A, Avis W, Bruckbauer J, Edwards P R, Hourahine B, Kraeusel S, Kusch G, Johnston R, Naresh-Kumar G, Martin R W, Nouf-Allehiani M, Pascal E, Spasevski L, Thomson D, Vespucci S, Parbrook P J, Smith M D, Enslin J, Mehnke F, Kneissl M, Kuhn C, Wernicke T, Hagedorn S, Knauer A, Kueller V, Walde S, Weyers M, Coulon P-M, Shields P A, Zhang Y, Jiu L, Gong Y, Smith R M, Wang T and Winkelmann A 2019 Scanning electron microscope as a flexible tool for investigating the properties of UV-emitting nitride semiconductor thin films. *Photonics Res.* **7** B73-82
[46] Jablon B M, Mingard K, Winkelmann A, Naresh-KumarG , Hourahine B and Trager-Cowan C 2020 Subgrain structure and dislocations in WC-Co hard metals revealed by electron channelling contrast imaging. *Int. J. Refract. Met.* **87** 105159